MATERIALS SCIENCE

Pulsed transistor operation enables miniaturization of electrochemical aptamer-based sensors

Sophia L. Bidinger[1], Scott T. Keene[1,2], Sanggil Han[1], Kevin W. Plaxco[3], George G. Malliaras[1]*, Tawfique Hasan[1]*

By simultaneously transducing and amplifying, transistors offer advantages over simpler, electrode-based transducers in electrochemical biosensors. However, transistor-based biosensors typically use static (i.e., DC) operation modes that are poorly suited for sensor architectures relying on the modulation of charge transfer kinetics to signal analyte binding. Thus motivated, here, we translate the AC "pulsed potential" approach typically used with electrochemical aptamer-based (EAB) sensors to an organic electrochemical transistor (OECT). Specifically, by applying a linearly sweeping square-wave potential to an aptamer-functionalized gate electrode, we produce current modulation across the transistor channel two orders of magnitude larger than seen for the equivalent, electrode-based biosensor. Unlike traditional EAB sensors, our aptamer-based OECT (AB-OECT) sensors critically maintain output current even with miniaturization. The pulsed transistor operation demonstrated here could be applied generally to sensors relying on kinetics-based signaling, expanding opportunities for noninvasive and high spatial resolution biosensing.

INTRODUCTION

To address the challenge of signal amplification in electrochemical biosensors, there has been a trend toward transistor-based platforms that both transduce and amplify electrochemical signals. Among these, organic electrochemical transistors (OECTs) have emerged as a particularly high-performance candidate due to the large signal gain associated with volumetric ion penetration throughout a conducting polymer channel, commonly composed of the commercially available blend poly(3,4ethylenedioxythiophene) doped with poly (styrene sulfonate) (PEDOT:PSS) (*1*). By amplifying directly at the sensing location, these systems have been shown to afford better signal-to-noise ratios than simple electrode-based approaches when used, for example, in neural recordings (*2*). OECTs have also been applied to a variety of electrochemical sensing approaches, typically by integrating a biorecognition element at the gate electrode. For example, OECT glucose sensors have been demonstrated in which glucose oxidase is immobilized on a gate electrode such that changes in glucose concentration modulate the source-drain current (I_D) (*3*, *4*). Alternatively, gate voltage shifts have also been used to monitor analyte binding in transistor-based biosensors (*5*). All of these applications, however, use direct current (DC) methods. This works well for systems that supply a continuous signal that is proportional to the analyte concentration (e.g., the current produced by enzyme-based sensors, the potentials produced on ion-selective membranes, etc.). However, an important, emerging class of biosensors instead relies on changes in charge transfer rate (k_{CT}), a signal transduction mechanism that is difficult to monitor effectively using DC methods (*6*).

Among biosensors that use binding-induced changes in electron transfer kinetics, electrochemical aptamer-based (EAB) sensors are rapidly growing in importance because of their versatility and their exceptional selectivity (*7*–*10*). In these sensors, an aptamer (a DNA or RNA molecule selected in vitro to bind to a specific molecular target) is first reengineered such that target binding causes it to undergo a conformational change (*11*). The aptamer is then modified with a thiol linker for immobilization onto a gold electrode. The opposite end of the aptamer is attached to a redox reporter (typically methylene blue) to generate an electrochemical signal that is independent of any redox activity of the analyte. By altering the distance between the redox reporter and the underlying electrode, the aptamer's binding-induced conformational change modulates the rate of electron transfer to the electrode (Fig. 1) (*12*), which can be monitored using a variety of transfer kinetics–sensitive electrochemical methods (*11*, *13*). AC voltammetry, for example, interrogates these sensors using a sinusoidal waveform with a frequency corresponding to the charge transfer rate of interest. The amplitude of the resulting current then depends on the average transfer rate of the redox reporter, thus reporting on the fraction of the aptamers that are target bound (*13*). Because it is even more sensitive to changes in transfer rate, however, square-wave voltammetry (SWV) is now the most commonly used approach to interrogate EAB sensors (*10*). This technique uses a square pulse superposed over a linearly sweeping voltage, with the pulse length being tuned to the frequency (transfer rate) of interest and the current being sampled only at the end of each pulse, rendering it particularly sensitive to transfer rates. EAB sensors using SWV interrogation have been shown to support continuous molecular monitoring in situ in the body, including in real-time monitoring of pharmacokinetics and metabolism in awake animals (*14*) and closed-loop feedback control over plasma drug levels (*15*).

Because of the small currents produced by surface-bound aptamers, an increasingly important limitation of traditional (electrode-based) EAB sensors is the difficulty of miniaturizing them below their current, few-millimeter length scales (*16*). In response, earlier works have attempted to amplify EAB sensors via OECT-based platforms, but the existing DC transistor sensing methods are not particularly sensitive to changes in electron transfer kinetics, rendering them suboptimal for this application (*17*, *18*). Here, however, we adapt square-wave voltage operation at the gate electrode of an OECT to amplify the signals produced by EAB sensors. The resulting amplification

[1]Electrical Engineering Division, Department of Engineering, University of Cambridge, 9 JJ Thomson Ave., Cambridge CB3 0FA, UK. [2]Department of Physics, University of Cambridge, Cambridge CB3 0FA, UK. [3]Department of Chemistry and Biochemistry and Biological Engineering Program, University of California Santa Barbara, Santa Barbara, CA 93106, USA.
*Corresponding author. Email: gm603@cam.ac.uk (G.G.M.); th270@cam.ac.uk (T.H.)

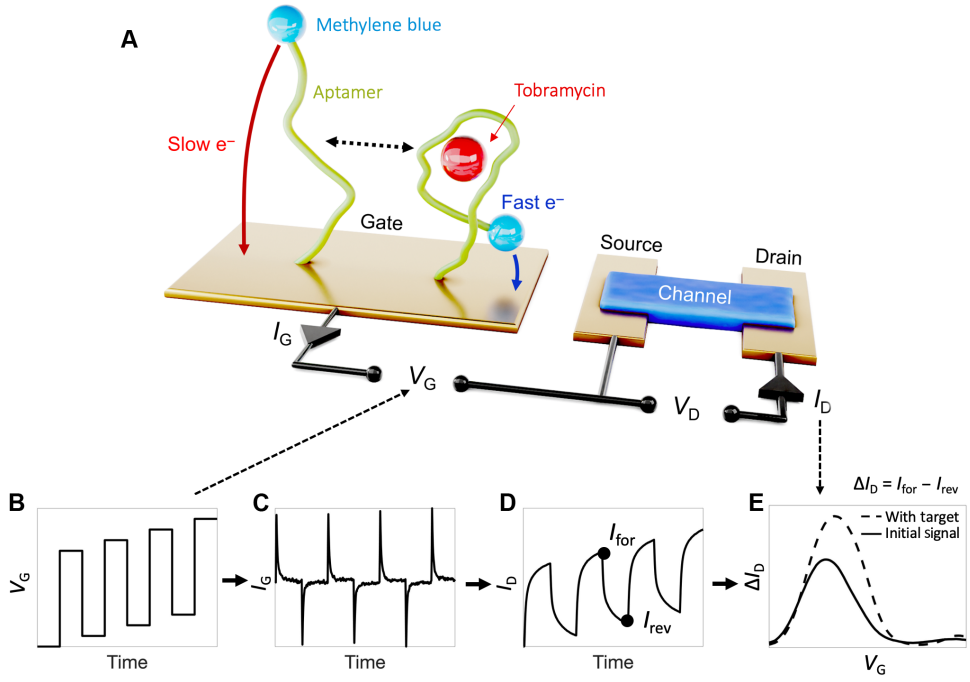

Fig. 1. Square-wave gate potential profiles support high-gain aptamer-based OECT sensing. (**A**) Schematic of the aptamer-based OECT, which includes methylene blue–modified aptamers immobilized on the gate electrode. This functionalized planar gold gate and the PEDOT:PSS channel are designed to match capacitance allowing for voltage drop at both the channel and gate sides. (**B**) A pulse square wave superimposed over a voltage sweep is input as V_G, yielding (**C**) I_G current decays from the oxidation of the methylene blue. (**D**) The resulting I_D is proportional to integrated I_G. (**E**) Measuring the difference between each forward and reverse pulse current then yields a distinct methylene blue redox peak. Upon target addition, the charge transfer rate increases, yielding a larger integrated current and leading to a higher ΔI_D redox peak.

is scalable, with two orders of magnitude improvement for planar 0.13-mm^2 electrodes, suggesting that our approach will enable sensing at high spatial resolution in the mapping of molecular analyte concentrations.

RESULTS

EAB sensors typically use a three-electrode setup in which a specific voltage (relative to a reference electrode) is applied to the aptamer-functionalized working electrode, and the resulting Faradaic (redox-reaction-derived) current flowing to a separate counter electrode is measured. As noted, the transfer kinetics associated with this Faradaic current are typically measured using SWV. In this technique, each square voltage pulse drives a current transient decay. By sampling the current at the end of the pulse (the length of which is defined by the square-wave frequency), the measured current will be monotonically related to the charge transfer kinetics of the redox reporter. To optimize this strategy, the square-wave frequency is tuned to best distinguish between the transfer kinetics of the aptamer's bound and unbound states (*11*). The resulting current is correlated to the fraction of aptamers that are target bound, thus reporting on the concentration of the target.

We construct aptamer-based OECT (AB-OECT) sensors such that the target-recognizing aptamers are immobilized on the gate electrode (Fig. 1A). Rather than directly measuring the resulting Faradaic current at the gate, however, our approach uses the gate current to modulate the conductivity in the OECT channel. Specifically, the gate current drives ions from the electrolyte into and out of the conducting polymer channel, thereby modulating the charge carrier density (i.e., dedoping/doping). Thus, square-wave operation of OECTs is similar to square-wave operation of electrode-based sensors but with an additional amplification step. In adapting SWV to transistor-based sensors, we apply a square-wave gate voltage (V_G) sweep (Fig. 1B) that yields gate current (I_G) transients (Fig. 1C) caused by electron transfer to or from the methylene blue redox reporter. The OECT amplifies this gate current through the subsequent modulation in source-drain current (I_D; Fig. 1D), which is proportional to the integrated gate current

$$\Delta I_D = \frac{\mu}{L^2} V_D \int I_G \, dt \quad (1)$$

Here, μ is the hole mobility and W, d, and L are the channel width, thickness, and length, respectively (*19*). The redox peak is constructed from the differences between I_D sampled at times corresponding to the end of each V_G pulse ($I_{for} - I_{rev}$; Fig. 1D), and the relative peak height reports on the analyte concentration (Fig. 1E). It should be noted that, despite this extra amplification step, the interrogation times of both AB-OECTs and of traditional electrode EAB sensors remain limited by the charge transfer kinetics of the aptamer. Given this, translation to the OECT platform does not significantly change temporal resolution.

The gate-to-channel modulation that drives AB-OECT sensors can be represented by a simple circuit consisting of two capacitors in series, with C_G representing the gate capacitance and C_{CH} denoting the channel capacitance (fig. S1A). To maintain equilibrium across the circuit, the current flowing at the gate (in response to the redox reactions occurring on it) results in an equivalent charging of the channel ($Q_G = Q_{CH}$). Such behavior is not usually captured in

standard DC OECTs, which are instead designed to maximize voltage drop at the channel side ($C_G >> C_{CH}$) so that the transconductance [i.e., voltage-to-current gain (g_m)] is maximized. Instead, in our case, we use the current gain (β) of the OECT to amplify the redox current at the gate

$$\beta = \frac{\Delta I_D}{\Delta I_G} \quad (2)$$

To optimize the signal transduced by the AB-OECT, we empirically "tune" the gate-to-channel area ratio. This analysis indicates that a ratio of ~80, which corresponds to $C_G \approx C_{CH}$, is optimal (fig. S1B). That is, while lower ratios increase the voltage drop at the gate, increasing the driving force for Faradaic reactions, they also yield lower overall gate currents owing to the reduced number of redox molecules on the smaller electrode surface. In contrast, higher ratios result in too low a voltage drop at the gate to drive the Faradaic reaction as well as increase the background signal from the charging of the electric double layer at the electrode surface, lowering the overall signal-to-noise ratio. Of note, both the device geometry and the drain voltage magnitude affect the redox peak position, which is effectively being referenced against the PEDOT:PSS channel (*5*).

As our testbed to compare our AB-OECT sensors with the traditional, electrode-based platform, we focused on sensors using an aptamer that binds the antibiotic tobramycin. In the absence of this drug, the methylene blue on the aptamer is held relatively far from the electrode surface, yielding a relatively slow charge transfer rate (i.e., small k_{CT}). Upon binding the drug, in contrast, the aptamer folds into a configuration that brings the redox reporter closer to the electrode, increasing k_{CT}. Of note, for the electrode-based system, it is possible to select square-wave frequencies at which the redox peak responds to rising target concentrations by either increasing ("signal-on behavior," which is seen at square-wave frequencies that preferentially signal the bound state; see Fig. 2A) or decreasing ("signal-off behavior," preferentially signaling the unbound state) (*20*). In an OECT-based sensor, however, I_D is proportional to the integral of the current transient, and thus, the signal increases with increasing target concentration irrespective of the frequency used. Specifically, we have empirically found that the maximum signal gain (i.e., maximum relative difference between the bound and unbound states) saturates around 70 Hz (Fig. 2B). At lower frequencies, the sampled current has nearly completely decayed. We suggest that the lower resulting signal, which is also sampled over a longer period, might be the reason for the larger error at low frequencies. The overall frequency response is consistent with a simple simulated model of the AB-OECT system using measured aptamer site density taken from cyclic voltammetry (fig. S2) and using k_{CT} and OECT governing equations obtained from previous literature (fig. S3) (*14*, *19*). Further description of this model is included in text S1.

The previously reported benefits of EAB sensors are maintained when the approach is adapted to the OECT platform. For example,

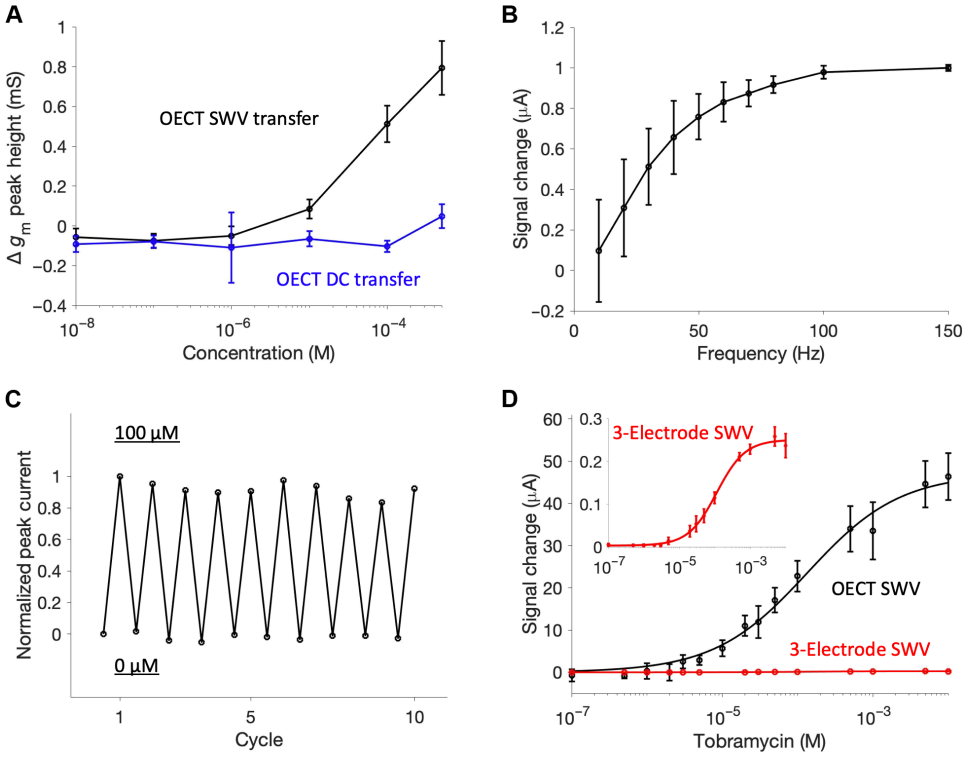

Fig. 2. Characterization of AB-OECT sensors. (**A**) AB-OECT sensing behavior showing g_m peak height growth with concentration using the square-wave OECT operation. The DC transfer curves do not respond to changes in analyte concentration. (**B**) Signal gain upon 1 mM tobramycin addition versus frequency saturates at approximately 70 Hz. (**C**) Peak signal change with 10 spike and rinse cycles indicates good reversibility. (**D**) Using identically sized gate and working electrodes (area = 0.79 mm^2), calibration curves generated using the OECT current are amplified significantly versus those generated using the three-electrode SWV. For example, at saturated target concentrations, the OECT signal is amplified by nearly 200-fold relative to the current seen when an identical device is interrogated using the standard, three-electrode configuration. Error bars correspond to the SD from replicate devices ($N = 3$). All data in this figure were measured in 1× PBS at ambient temperature. The OECT measurements used $V_D = -200$ mV.

the excellent reversibility of EAB sensors holds for their OECT implementation (Fig. 2C). Specifically, the normalized peak current after 10 spike and rinse cycles is within 3% of the original seen in the absence of target. Similarly, both the electrode and OECT system exhibit Langmuir-Hill isotherm binding performance (Fig. 2D) with low measurement variation shown in fig. S4. The expected isotherm (i.e., saturable) binding has not been demonstrated with DC OECT operation of EAB sensors, which may be more sensitive to pH and ionic concentration variation preventing signal saturation. Critically, the concentration-dependent peak height extracted by the AC OECT operation is specific to the electrochemical activity of the aptamer. A validation of the AB-OECT's specific response after fluctuating ionic concentration is shown in fig. S5. Because of this aptamer-specific signal, it is suitable for application in complex in vivo environments where selectivity is paramount. To further validate this selectivity, we challenged our device in defibrinated horse blood, where its response was quite similar to that seen in simple buffer systems (Fig. 3A). As with the traditional electrode platform, there is some signal drift in whole blood shown also in spike and rinse cycles (fig. S6). To ameliorate this, drift correction strategies such as kinetic differential measurements, which are commonly used with in vivo EAB sensors, should be considered for future in vivo AB-OECT measurements (*21*).

A major advantage of applying OECTs in EAB sensors is the ability to maintain an amplified signal even upon substantial miniaturization. The issue is that, in a three-electrode system, the signal shrinks proportionally to the reduced electrode area as the electrode accommodates fewer aptamers yielding less absolute current. While I_G is similarly reduced in smaller OECTs, due to its lower volume, a smaller channel requires proportionally less current to modulate a change in I_D (Eq. 1). That is, as the devices shrink, relative OECT amplification increases and, with this, the absolute signal is maintained. Given this, the OECT-based sensor should yield a higher signal than the traditional three-electrode system for all electrodes below 56 mm^2 (Fig. 3B). We believe that this highly scalable amplification will allow for a range of sensing applications that were previously infeasible for EAB platforms. For example, miniaturization can enable more sensors per area, which will yield higher-resolution spatial measurement. Another potential benefit of signal amplification in vivo is the expansion of sensor lifetime, which is limited by signal drift in whole blood. This represents a major challenge in EAB development. The higher initial signal afforded by AB-OECTs could expand the lifetime of EAB sensors by vastly increasing the initial signal, leading to a longer period over which sufficiently high signal-to-noise ratio is maintained.

DISCUSSION

Beyond the potential future applications of miniaturized EAB sensors, the presented pulsed V_G technique can be applied generally to a wide range of transistor and biorecognition element pairings. For example, differential pulse voltammetry uses a similar waveform to SWV and is used to reduce the effects of capacitive charging and to enable species differentiation by narrowing peaks. While the OECT was selected in this work for its high signal gain and good biocompatibility, the concept is not limited to OECTs; it will operate with the same attributes for any transistor biosensor that signals via a redox event with binding-induced k_{CT} changes at the gate electrode. By interrogating charge transfer kinetics in this way, pulsed operation will bring the advantages of transistor-derived amplification to a wide range of biosensor approaches.

MATERIALS AND METHODS

OECTs were fabricated following a previously reported nanofabrication protocol (fig. S7) (*22*). First, photolithography with a negative photoresist, AZ nLOF 2035 (Microchemicals GmbH), was used to outline the interconnects and source, drain, and gate electrodes on clean glass substrates. Next, 5 nm of titanium and 100 nm of gold were deposited (Kurt J Lesker PVD-75) after oxygen plasma (Diener Electronic Femto) activation. Gold liftoff was achieved by soaking overnight in NI555 stripper (Microchemicals GmbH). Next, silane treatment was used for adhesion to the first of two chemical vapor deposited 2-μm parylene-C (PaC) layers (Specialty Coating Systems Inc.). An antiadhesive solution was spin-coated before the second PaC layer to enable peel-off. To expose the contact and channel areas, a second photolithography step was completed with a positive photoresist, AZ 10XT (Microchemicals GmbH), and samples were etched with a reactive ion etcher (Oxford 80 Plasmalab plus). The OECT gates and channels were separated by dicing to enable separation for PEDOT:

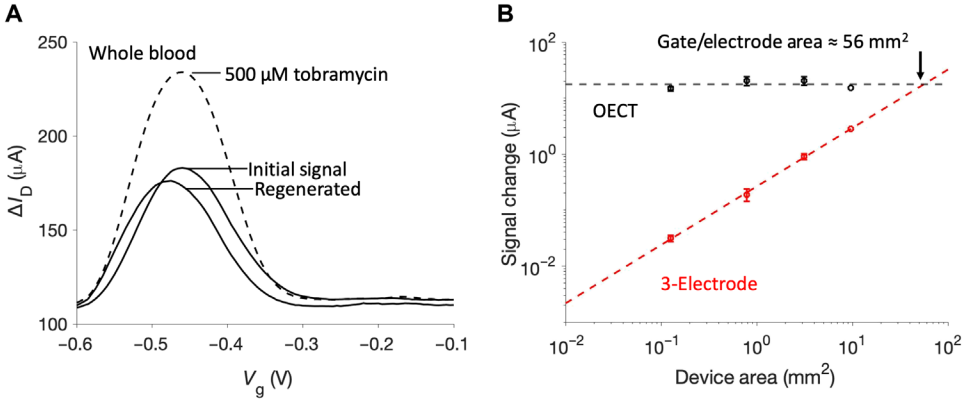

Fig. 3. AB-OECT sensors are suitable for in vivo amplification. (**A**) Signal peaks and reversible sensing performance are maintained in whole blood ($V_D = -300$ mV). (**B**) As devices are rescaled for miniaturization, OECT signal is maintained, while electrode current decreases linearly with area. Device area corresponds to both the working electrode and gate electrode areas, and OECT measurements used $V_D = -200$ mV and were performed in PBS. Error bars correspond to the SD from replicate devices ($N = 3$ for each of the three smallest areas and $N = 1$ for the largest area).

PSS spin coating. Ethylene glycol (5%, v/v) and 4-dodecylbenzenesulfonic acid (0.25%, v/v) were sonicated with PEDOT:PSS. Next, 1% (v/v) of (3-glycidyloxypropyl)trimethoxysilane was added, and the solution was passed through 0.45-μm polytetrafluoroethylene filters. Following another oxygen plasma treatment, two layers of the PEDOT:PSS mixture were spin-coated on the channels for 30 s at 3000 RPM. The sacrificial PaC layer was peeled off, and the samples were hard-baked to cross-link the PEDOT:PSS. Last, the samples were soaked in deionized water overnight and preconditioned to maximize stability (*23*).

The aminoglycoside aptamer [5′-HO-$(CH_2)_6$-S-S-$(CH_2)_6$-GGGACTTGGTTTAGGTAATGA-GTCCC-O-CH_2-$CHCH_2$OH-$(CH_2)_4$-NH-CO-$(CH_2)_2$-methylene blue-3′] was purchased from Sangon Biotech and used as supplied. A 2-μl aliquot of 100 μM aptamer in 1X phosphate buffered saline (PBS, 137 mM NaCl, 2.7 mM KCl, 10 mM Na_2HPO_4, and 1.8 mM KH_2PO_4) was thawed and mixed with 4 μl of 10 mM tris(2-carboxyethyl)phosphine (Sigma-Aldrich) for 8 hours to reduce the disulfide bond. Next, the aptamer solution was diluted to 500 nM with PBS and placed in a polydimethylsiloxane (PDMS) well over plasma-activated gate (working) electrodes for an overnight immobilization. Next, electrodes were rinsed and placed in a 10 mM 6-mercapto-1-hexanol (Sigma-Aldrich) for 5 hours to passivate. Last, electrodes were rinsed with PBS and connected to channels via a PDMS well.

OECT measurements were collected using a Keysight B1500A semiconductor device analyzer. All OECT measurements used a V_G sweeping from −600 to −100 mV. Electrode measurements were carried out on an Autolab potentiostat (Metrohm) using the gate electrode as working electrode with Ag/AgCl reference and platinum counter electrodes. For square-wave measurements on both the OECT and electrode, a 5-mV step and 20-mV amplitude were used, as adapted from previous work on the aminoglycoside aptamer (*24*). Unless otherwise noted, OECT SWV measurements used a frequency of 70 Hz, and electrode SWV measurements used 240 Hz. Calibration curves were measured by adding successive graduated amounts of stock tobramycin (Thermo Fisher Scientific) in PBS. Measurements were recorded after 5 min of equilibration time. Reversibility was assessed by spiking with 100 μM of stock tobramycin, followed by triple rinsing with PBS. In each case of rinsing or tobramycin addition, measurements were recorded after a 5-min equilibrium period.

SUPPLEMENTARY MATERIALS

Supplementary material for this article is available at https://science.org/doi/10.1126/sciadv.add4111

REFERENCES AND NOTES

1. D. Khodagholy, J. Rivnay, M. Sessolo, M. Gurfinkel, P. Leleux, L. H. Jimison, E. Stavrinidou, T. Herve, S. Sanaur, R. M. Owens, G. G. Malliaras, High transconductance organic electrochemical transistors. *Nat. Commun.* **4**, 2133 (2013).
2. D. Khodagholy, T. Doublet, P. Quilichini, M. Gurfinkel, P. Leleux, A. Ghestem, E. Ismailova, T. Hervé, S. Sanaur, C. Bernard, G. G. Malliaras, In vivo recordings of brain activity using organic transistors. *Nat. Commun.* **4**, 1575 (2013).
3. H. Tang, F. Yan, P. Lin, J. Xu, H. L. W. Chan, Highly sensitive glucose biosensors based on organic electrochemical transistors using platinum gate electrodes modified with enzyme and nanomaterials. *Adv. Funct. Mater.* **21**, 2264–2272 (2011).
4. C. Liao, M. Zhang, L. Niu, Z. Zheng, F. Yan, Highly selective and sensitive glucose sensors based on organic electrochemical transistors with graphene-modified gate electrodes. *J. Mater. Chem. B* **1**, 3820–3829 (2013).
5. F. Torricelli, D. Z. Adrahtas, Z. Bao, M. Berggren, F. Biscarini, A. Bonfiglio, C. A. Bortolotti, C. D. Frisbie, E. Macchia, G. G. Malliaras, I. McCulloch, M. Moser, T.-Q. Nguyen, R. M. Owens, A. Salleo, A. Spanu, L. Torsi, Electrolyte-gated transistors for enhanced performance bioelectronics. *Nat. Rev. Methods Primers* **1**, 66 (2021).
6. A. M. Downs, J. Gerson, K. L. Ploense, K. W. Plaxco, P. Dauphin-Ducharme, Subsecond-resolved molecular measurements using electrochemical phase interrogation of aptamer-based sensors. *Anal. Chem.* **92**, 14063–14068 (2020).
7. F. Pfeiffer, G. Mayer, Selection and biosensor application of aptamers for small molecules. *Front. Chem.* **4**, 25 (2016).
8. A. M. Yoshikawa, A. Rangel, T. Feagin, E. M. Chun, L. Wan, A. Li, L. Moekl, D. Wu, M. Eisenstein, S. Pitteri, H. T. Soh, Discovery of indole-modified aptamers for highly specific recognition of protein glycoforms. *Nat. Commun.* **12**, 7106 (2021).
9. H. Abu-Ali, A. Nabok, T. J. Smith, Development of novel and highly specific ssDNA-aptamer-based electrochemical biosensor for rapid detection of mercury (II) and lead (II) ions in water. *Chemosensors* **7**, 27 (2019).
10. L. R. Schoukroun-Barnes, F. C. Macazo, B. Gutierrez, J. Lottermoser, J. Liu, R. J. White, Reagentless, Structure-switching, electrochemical aptamer-based sensors. *Annu. Rev. Anal. Chem.* **9**, 163–181 (2016).
11. R. J. White, K. W. Plaxco, Exploiting binding-induced changes in probe flexibility for the optimization of electrochemical biosensors. *Anal. Chem.* **82**, 73–76 (2009).
12. A. A. Lubin, K. W. Plaxco, Folding-based electrochemical biosensors: The case for responsive nucleic acid architectures. *Acc. Chem. Res.* **43**, 496–505 (2010).
13. R. J. White, N. Phares, A. A. Lubin, Y. Xiao, K. W. Plaxco, Optimization of electrochemical aptamer-based sensors via optimization of probe packing density and surface chemistry. *Langmuir* **24**, 10513–10518 (2008).
14. N. Arroyo-Currás, J. Somerson, P. A. Vieira, K. L. Ploense, T. E. Kippin, K. W. Plaxco, Real-time measurement of small molecules directly in awake, ambulatory animals. *Proc. Natl. Acad. Sci.* **114**, 645–650 (2017).
15. N. Arroyo-Currás, G. Ortega, D. A. Copp, K. L. Ploense, Z. A. Plaxco, T. E. Kippin, J. P. Hespanha, K. W. Plaxco, High-precision control of plasma drug levels using feedback-controlled dosing. *ACS Pharmacol. Transl. Sci.* **1**, 110–118 (2018).
16. A. M. Downs, J. Gerson, M. N. Hossain, K. Ploense, M. Pham, H.-B. Kraatz, T. Kippin, K. W. Plaxco, Nanoporous gold for the miniaturization of in vivo electrochemical aptamer-based sensors. *ACS Sens.* **6**, 2299–2306 (2021).
17. Y. Liang, C. Wu, G. Figueroa-Miranda, A. Offenhäusser, D. Mayer, Amplification of aptamer sensor signals by four orders of magnitude via interdigitated organic electrochemical transistors. *Biosens. Bioelectron.* **144**, 111668 (2019).
18. N. Saraf, E. R. Woods, M. Peppler, S. Seal, Highly selective aptamer based organic electrochemical biosensor with pico-level detection. *Biosens. Bioelectron.* **117**, 40–46 (2018).
19. J. T. Friedlein, R. R. McLeod, J. Rivnay, Device physics of organic electrochemical transistors. *Org. Electron.* **63**, 398–414 (2018).
20. P. Dauphin-Ducharme, K. W. Plaxco, Maximizing the signal gain of electrochemical-DNA sensors. *Anal. Chem.* **88**, 11654–11662 (2016).
21. K. K. Leung, A. M. Downs, G. Ortega, M. Kurnik, K. W. Plaxco, Elucidating the mechanisms underlying the signal drift of electrochemical aptamer-based sensors in whole blood. *ACS Sens.* **6**, 3340–3347 (2021).
22. A. G. Polyravas, V. F. Curto, N. Schaefer, A. B. Calia, A. Guimera-Brunet, J. A. Garrido, G. G. Malliaras, Impact of contact overlap on transconductance and noise in organic electrochemical transistors. *Flex. Print. Electron.* **4**, 044003 (2019).
23. S. L. Bidinger, S. Han, G. G. Malliaras, T. Hasan, Highly stable PEDOT:PSS electrochemical transistors. *Appl. Phys. Lett.* **120**, 073302 (2022).
24. L. R. Schoukroun-Barnes, S. Wagan, R. J. White, Enhancing the analytical performance of electrochemical RNA aptamer-based sensors for sensitive detection of aminoglycoside antibiotics. *Anal. Chem.* **86**, 1131–1137 (2014).

Acknowledgments: We acknowledge figure preparation support from R. Mizuta and G. Bae. We acknowledge A. Downs for consultations and guidance regarding EAB sensors. **Funding:** S.L.B. acknowledges funding from the Cambridge International & Churchill Pochobradsky Scholarship. S.T.K. acknowledges funding from the European Union's Horizon 2020 research and innovation programme under the Marie Skłodowska-Curie grant agreement no. 101022365. S.H. was supported by the Natural Environment Research Council (NERC) under award no. NE/T012293/1. The authors acknowledge funding from the Engineering and Physical Sciences Research Council (EP/W017091/1) and (EP/L016087/1). **Author contributions:** The project was initially conceptualized by S.L.B., G.G.M., and K.W.P. Device fabrication and development were carried out by S.L.B., S.H., and S.T.K. Experiments were designed and analyzed by T.H., S.L.B., and S.T.K. S.L.B. prepared the manuscript and figures. K.W.P., G.G.M., S.T.K., and T.H. contributed to the writing of the manuscript. T.H., G.G.M., and K.W.P. oversaw the project. **Competing interests:** The authors declare that they have no competing interests. **Data and materials availability:** All data needed to evaluate the conclusions in the paper are present in the paper and/or the Supplementary Materials. Supporting information on device geometry, packing density measurement, frequency gain fitting, ionic selectivity, and fabrication protocol is available in the supplementary materials.

Submitted 9 June 2022
Accepted 28 September 2022
Published 16 November 2022
10.1126/sciadv.add4111